Journal of Molecular Structure 1327 (2025) 141121

Contents lists available at ScienceDirect

Journal of Molecular Structure

journal homepage: www.elsevier.com/locate/molstr

Structural, Hirshfeld surface and nonlinear optical properties of 4-fluorobenzylidene-4-methoxyaniline (FBMOA) and 4-fluorobenzylidene-4-methylaniline (FBMA)

A. Subashini [a,*], R. Kumaravel [b], Helen Stoeckli-Evans [c], T. Sabari Girisun [d], Sharon Mary Tomson [e], Reji Philip [e], Aurelien Crochet [f], R. Ramesh Babu [g], K. Ramamurthi [g]

[a] PG and Research Department of Physics, Srimad Andavan Arts and Science College (Autonomous), Affliated to Bharathidasan University, Tiruchirappalli 620 005, India
[b] Department of Physics, Annapoorana Engineering College (Autonomous), Salem 636 308, Tamilnadu, India
[c] Institute of Physics, University of Neuchâtel, Rue Emile-Argand 11, CH-2000 Neuchâtel, Switzerland
[d] Nanophotonics Laboratory, School of Physics, Bharathidasan University, Tiruchirappalli 620 024, India
[e] Ultrafast and Nonlinear Optics Laboratory Raman Research Institute, C. V. Raman Avenue, Sadashivanagar, Bangalore 560 080, India
[f] Chemistry Department, University of Fribourg, Chemin du Musee 9, CH-1700 Fribourg, Switzerland
[g] Crystal Growth and Thin Film Laboratory, Department of Physics, Bharathidasan University, Tiruchirappalli 620 024, India

ARTICLE INFO

Keywords:
N-benzylideneaniline
Organofluorine
Crystal structure
Hirshfeld surface
2D-fingerprint plots
Optical limiting properties

ABSTRACT

In the present work the syntheses, molecular structures and properties of two novel Schiff base N-benzylideneanilines, 4-fluorobenzylidene-4-methoxyaniline (FBMOA) and 4-fluorobenzylidene-4-methylaniline (FBMA), are described. Their structures were confirmed by spectral and crystallographic analyses. FBMA crystallizes with two independent molecules in the asymmetric unit. The interatomic interactions in the crystals of FBMOA and FBMA, that contain different substituents, were investigated through Hirshfeld surface analysis. Thermally, FBMOA and FBMA were found to be stable; FBMOA undergoes bulk decomposition at ~ 180 °C and FBMA at ~230 °C. UV–vis-NIR spectroscopy and open-aperture Z-scan studies were employed to characterize the linear and nonlinear optical behavior of the two compounds. Their structures and properties are compared to those of similar organo halide-substituted Schiff base compounds.

1. Introduction

Organic materials have been extensively explored as nonlinear optical (NLO) materials to enhance two photon absorption cross-sections [1], making them suitable for optoelectronic and photonic devices [2–4]. Organic Schiff bases have been found to promote high NLO properties due to their mesomeric effect [5,6], which enhances the delocalization of electrons, thereby increasing the NLO response of the molecule. Substituents in the *para* and *meta* positions of benzylideneaniline (NBA) Schiff bases have a greater influence on the C = N bond of the benzylidene ring compared to the aniline ring [7]. The strength of the intramolecular bonding is dependent on the nature of the substituents on both aromatic rings [8]. Organofluorine compounds, that feature a C-F bond, are notably more stable than those featuring a C—H or other C-heteroatom bonds. This enhanced stability arises from fluorine's high electronegativity, strong bond strength, oxidative resistance and its unique surface properties [9].Moreover, their low photon absorption,combined with high pharmacological activity, chemical stability and thermal resilience, make organofluorine compounds essential in a wide range of applications. For example, surfactants, refrigerants, ion-exchange membranes, and optical fibers [9,10]. Many recent reports are available on related NBA Schiff base compounds [11–19]. An overview of Schiff bases in organic, inorganic and physical chemistry has been published recently [20]. Two previously reported compounds, 4-chlorobenzylidene)-4-methoxyaniline (CBMOA) and 4-bromobenzylidene-4-methoxyaniline (BBMOA), were synthesized using 4-methoxyaniline as a starting material. Their crystal structures [21,22] and non-linear optical properties [18,19] have been reported. In the present work, 4-fluorobenzylidene-4-methoxyaniline (FBMOA) and 4-fluorobenzylidene-4-methylaniline (FBMA) were synthesized using as

* Corresponding author.
E-mail address: viji.suba@gmail.com (A. Subashini).

https://doi.org/10.1016/j.molstruc.2024.141121
Received 28 September 2024; Received in revised form 27 November 2024; Accepted 15 December 2024
Available online 20 December 2024

Table 1
Crystallographic and refinement details for FBMOA and FBMA.

Compound Name	FBMOA	FBMA
Molecular Formula	C_{14} H_{12} F N O	C_{14} H_{12} F N
Formula Weight [g/mol]	229.25	213.25
Crystal Size [mm]	0.25×0.33×0.45	0.46×0.69×0.99
Crystal System	Monoclinic	Monoclinic
Space group	Cc	$P2_1/c$
a [Å]	24.700 (2)	11.5538 (4)
b[Å]	7.2672 (5)	13.5615 (5)
c [Å],	6.3566 (6)	14.5216 (4)
α (°), β (°), γ (°)	90, 90.277 (7), 90	90, 90.072(2), 90
V [Å ^{3}]	1140.97 (16)	2275.34 (13)
Z, Z'	4, 1	8, 2
Temperature [K]	173	250
Wavelength [Å]	0.71073	1.54186
D(calc) [g/cm^3]	1.334	1.245
μ [mm^{-1}], T_{min}/T_{max}	0.095, 0.867/1.000	
μ [mm^{-1}], T_{min}/T_{max}		0.084, 0.510/0.734
F(000)	480	896
θ Min-Max [°]	1.65, 25.63	6.92, 67.99
Dataset ±*h*; ±*k*; ±*l*	-29, 30; -8, 8; -7, 7	-13, 13; -16, 15; -12, 16
Total, Uniq. Data, R(int)	7578, 2099, 0.033	49,061, 4053, 0.078
Observed data [$I > 2.0\ \sigma(I)$]	1760	3865
N_{ref}, N_{par}	2099, 156	4053, 293
R, wR2, S	0.0335, 0.0767, 1.03	0.0756, 0.2116, 1.06
Min. and Max. Resd.Dens. [e/Å^3]	-0.16, 0.16	-0.40, 0.47

reactants 4-methoxyaniline for FBMOA and 4-methylaniline for FBMA. They were characterized by their structural, optical, nonlinear optical, spectral and thermal properties. In the presence of different electron-withdrawing groups (F, Cl, Br) on the aldehyde moiety in FBMOA, CBMOA, and BBMOA, the electron density distribution within their molecules varies. This variation leads to differences in how these molecules pack in the solid state. Furthermore, this work compares and presents the influence of methoxy and methyl groups on the aniline rings of FBMOA and FBMA, as these groups act as electron-donating substituents.

2. Experimental section

2.1. Synthesis and crystal growth

The experimental procedure to synthesize FBMOA and FBMA followed the same procedure previously reported for CBMOA and BBMOA [18,19]. The title compounds were prepared by dissolving a 1:1 molar ratio of 4-methoxyaniline or 4-methylaniline, respectively, with 4-fluorobenzaldehyde in ethanol. The resultant solution was heated under reflux at 70 °C for 8 h The precipitated products were obtained when the mixture was cooled to room temperature. They were purified by repeated recrystallization in methanol. Purified FBMOA and FBMA were then dissolved in methanol and ethanol, respectively. Slow evaporation of these solutions at room temperature yielded crystals suitable for X-ray diffraction analysis.

2.2. X-ray diffraction

The data collection for FBMOA was performed at 173 K using a Stoe Mark II-Image Plate diffractometer [23], while for FBMA data were collected at 250 K using a STOE STADIVARI diffractometer [23]. For the FBMOA crystal, the program SHELXS-97 [24] was used to solve the structure by direct methods and SHELXL-2019/3 [25] was used for refinement and all further calculations. PLATON's MULABS routine [26], which employs a multi-scan approach, was used for a semi-empirical absorption correction. The crystal structure of FBMA was solved with the Olex2 software's structure solution program olex2.solve using Charge Flipping [27]. Refinement was performed using the Olex2.refine package [28], which employs Gauss-Newton minimization. FBMA crystallizes in the space group $P2_1/c$, with two independent molecules in the asymmetric unit ($Z = 8$, $Z' = 2$). The crystal was twinned with matrix -1 0 0, 0 -1 0, 0 0 1 and refined as a two-component twin with a Batch Scale Factor (BASF) of 0.494. Crystallographic details for both compounds are given in Table 1. Figures were drawn using the program Mercury [29].

2.3. Hirshfeld surface analysis

Crystal Explorer17 [30] was employed to perform Hirshfeld surface (HS) analysis to investigate the interatomic interactions present in the crystals of FBMOA and FBMA. The HS surfaces are mapped according to the colour ranges -0.044 to 1.137 a.u. and -0.023 to 1.491 a.u., respectively. They are compared to those of BBMOA and CBMOA (in the colour ranges -0.091 to 1.135 and 0.145 to -1.028 a.u., respectively).

2.4. Fourier transform infrared spectral analysis

A PerkinElmer Paragon 500, a Fourier transform infrared (FTIR) spectrometer, was used to collect the infrared spectrum (400 – 4000 cm^{-1}) of FBMOA and FBMA using the KBr pellet technique.

2.5. Thermal analyses

Thermogravimetric (TG) and Differential thermal (DT) analyses were carried out employing an SDT Q600 V20.9 Build 20 S. T. A - 1500 Simultaneous Thermo Analytical system across the temperature range 30 - 300 °C and HITACHI STA300 for FBMA in the temperature range 30 - 500 °C. Analyses were carried out under a nitrogen atmosphere at a heating rate of 10 °C/min. Samples of 1.52 mg (FBMOA) and 3.002 mg (FBMA) were taken in alumina crucible for measurement.

2.6. Linear and nonlinear optical properties

The optical absorption characteristics of compounds FBMOA and FBMA were analyzed in the range of 200 – 1100 nm, employing a Varian Cary 5E UV–vis-NIR spectrophotometer.

Nonlinear absorption in FBMOA and FBMA were measured by employing the mono beam Z-scan open aperture technique using an Nd: YAG laser which produces 532 nm, 5 ns (FBMOA) and 9 ns (FBMA) laser pulses. Two lenses were used to focus the laser beam: a 10 cm focal length lens for FBMOA and a 15 cm focal length lens for FBMA, and the radius of the beam at the focus was 17 μm. The energy of the laser pulses was 70μJ (FBMOA) and 100μJ (FBMA). The samples were each dissolved in chloroform and taken in 1 mm path length quartz cells. The linear transmission of the solution was 88%. Each prepared sample was translated along the beam axis from one side of the focus to the other (the focal point is taken as $Z = 0$) and the sample transmission was measured at various positions with respect to the focus. The laser beam exhibits a maximum energy density at its focal point. This density decreases symmetrically in both directions along the beam axis. From the measurements, the sample transmission (T) can be plotted as a function of the sample position (Z), which gives the Z-scan curve. The Z-scan curves can be numerically fitted to Eq. (1) [31]

$$T = \left(\frac{(1-R)^2\exp(-\dot{\alpha}L)}{\sqrt{\pi q_o}}\right)\int_{-\infty}^{\infty} In\sqrt{1+q_o\exp(-t^2)}dt \quad (1)$$

Where L = sample length, R = sample reflectivity, t = laser pulse duration (full width at half maximum), and ά = linear absorption coefficient. q_o is given by $\beta(1\text{-}R)I_oL_{eff}$, where $L_{eff}=(1\text{-}\exp(\acute{\alpha}L))/\acute{\alpha}$, and β = effective third order nonlinear absorption coefficient. In the present case, two photo absorption (TPA) is the major contributor to nonlinear absorption. The TPA process can be written as $\beta I = \sigma N(I)$, where σ is the Excited state absorption (ESA) cross section, and N(I) is the intensity dependent excited state population density.

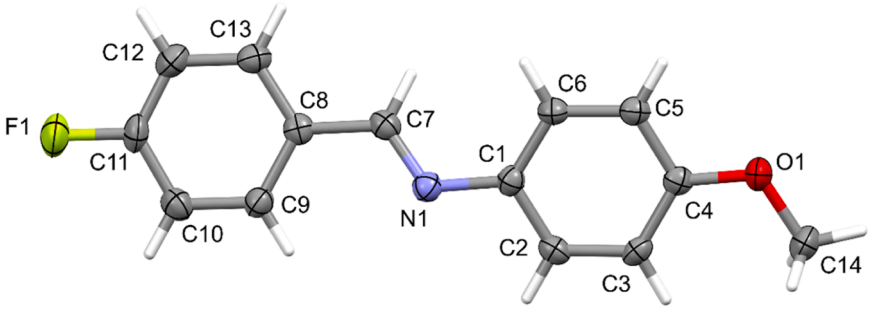

Fig. 1a. The molecular structure of FBMOA, with displacement ellipsoids drawn at the 50% probability level.

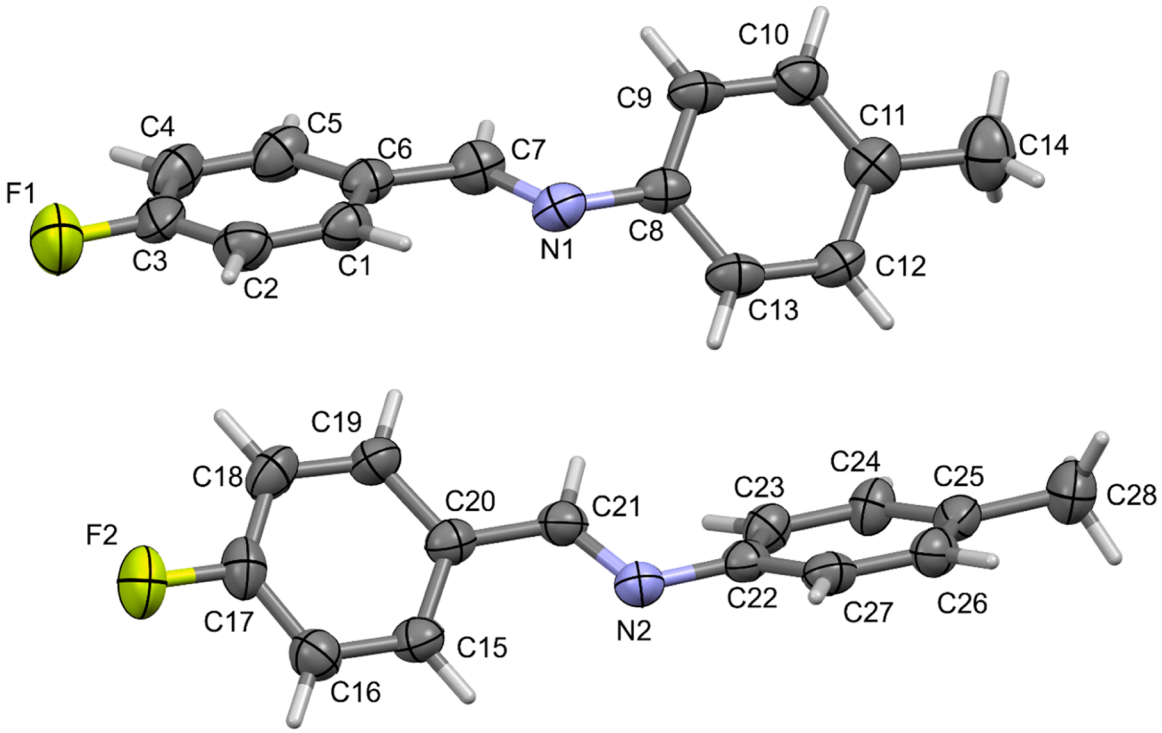

Fig. 1b. The molecular structure of the two independent molecules of FBMA (**1**-F1, **2**-F2), with displacement ellipsoids drawn at the 50% probability level.

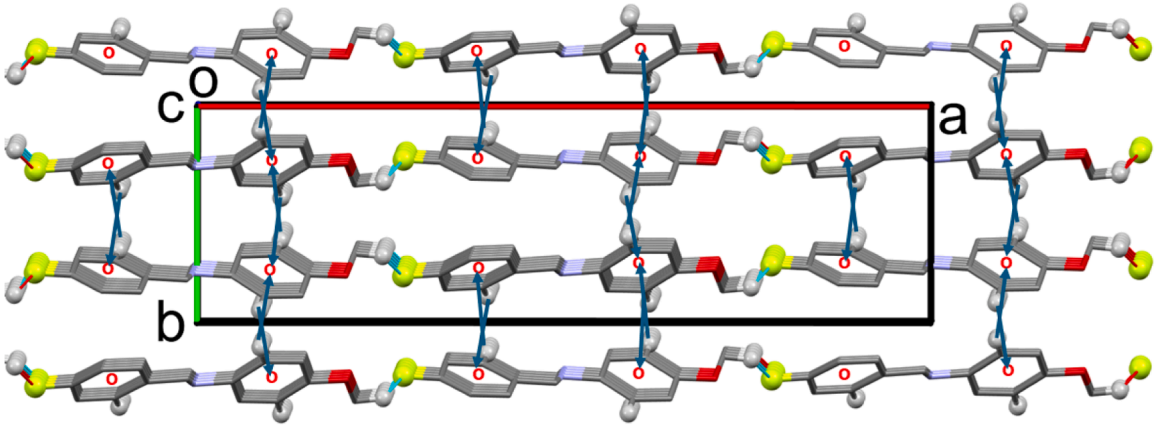

Fig. 2a. The crystal packing of FBMOA viewed along the *c*-axis direction. For clarity, only the H atoms (grey balls) involved in C—H…F and C—H…π interactions (green arrows; centroid red ring) have been included. The C—H…F hydrogen bond is shown as a cyan dashed line.

Table 2a
Hydrogen bonding and C—H…π interactions (Å, °) in the crystal of FBMOA.

D—H···*A*	*D*—H	H···*A*	*D*···*A*	*D*—H···*A*
C14—H14*C*···F1^{i}	0.98	2.55	3.147 (3)	119
C3—H3···*Cg*1^{ii}	0.95	2.80	3.591 (3)	141
C6—H6···*Cg*1^{iii}	0.95	2.73	3.534 (3)	143
C9—H9···*Cg*2^{ii}	0.95	2.99	3.658 (3)	129

Cg1 and Cg2 are the centroids of rings C1-C6 and C8-C13, respectively.
Symmetry codes: (i) $x+1/2, -y+1/2, z+3/2$; (ii) $x, -y, z+1/2$; (iii) $x, -y+1, z-1/2$.

3. Results and discussion

3.1. Crystal and molecular structures

The molecular structure of FBMOA is illustrated in Fig. 1a. The molecule is relatively planar with the aromatic rings (C1-C6 and C8-C13) being inclined to each other by only 8.91(15)°. Compound FBMA crystallizes with two independent molecules (1 and 2) in the asymmetric unit, as shown in Fig. 1b. The molecular overlap of inverted molecule 2 on molecule 1 of FBMA, has an r.m.s. deviation of 0.048 Å and a maximum deviation of 0.076 Å (Mercury [19]). The overlap of the two molecules is shown in Figure S1 of the Supplementary information. In molecule 1 of FBMA rings (C1 – C6) and (C8 – C13) are inclined to each other by 51.02(17)°, while in molecule 2 rings (C15 – C20) and (C22 – C27) are inclined to each other 55.74(17)°. Both compounds exhibit an *E* configuration around the C = N bond. In FBMOA this bond length [N1=C7] is 1.274(3) Å, while in FBMA the C = N bond lengths are 1.274 (4) Å [N1=C7] and 1.263 (4) Å [N2=C21]. A search of the Cambridge Structural Database (version 5.45, last update September 2024) [32] for *4/4′*-substituted benzylideneaniline Schiff bases yielded 241 purely organic compounds when applying the restrictions – only 3D co-ordinates, R factor </= 0.075, no disorder, no errors, no polymerics, no ions, and no powder diffraction studies. On analyzing various parameters using Mercury [29] it was found that the C = N bond length varies from 1.13 to 1.334 Å, with a mean value of 1.272 (11) Å. The values reported above for the C = N bond length in FBMOA *viz.*1.274 (3) Å, and 1.274 (3) and 1.263 (4) Å for FBMA, fall within these limits and are close to the mean value. For CBMOA [21] and BBMOA [22] the same bond lengths are both slightly shorter at 1.255(3) and 1.250(8) Å, respectively. The dihedral angle involving the two aromatic rings shows a small cluster about *ca*7.3°, similar to the value found for FBMOA (8.91 (15)°), and a larger cluster about *ca*52°, as seen for the two independent molecules of FBMA (51.02(7) and 55.74(17)°). The dihedral angle involving the two aromatic rings in CBMOA [21] and BBMOA [22] are 9.13(9) and 9.6(3)°, respectively, close to the value reported above for FBMOA.

The crystal packing of FBMOA, viewed along the *c*-axis direction, is illustrated in Fig. 2a. Hydrogen bonding and C—H…π interactions are given in Table 2a. Here, molecules are linked by three C—H…π interactions forming double-ribbon-like structures propagating along the *c*-axis direction. The double-ribbons are linked by C—H…F hydrogen bonds so forming a three-dimensional framework. The crystal packing of CBMOA [21] and BBMOA [22] also involve C—H…π interactions, but in the absence of C—H…Cl or C—H…Br hydrogen bonds form only ribbon-like structures.

The crystal packing of FBMA, viewed along the *b*-axis direction, is illustrated in Fig. 2b (a). The C—H…π interactions are given in Table 2b. The crystal packing as a result of the first three C—H…π interactions is

Table 2b
C—H…π interactions (Å) in the crystal of FBMA.

D—H···*A*	*D*—H	H···*A*	*D*···*A*	*D*—H···*A*
C4—H4···*Cg*2^{i}	0.94	2.89	3.493 (4)	123
C9—H9···*Cg*1^{ii}	0.94	2.89	3.648 (4)	139
C12—H12···*Cg*4	0.94	2.91	3.570 (3)	128
C16—H16···*Cg*4^{iii}	0.94	2.97	3.661 (4)	131
C18—H18···*Cg*1	0.94	2.97	3.564 (4)	122
C23—H23···*Cg*2^{iv}	0.94	2.67	3.451 (3)	141
C26—H26···*Cg*3^{v}	0.94	2.86	3.602 (3)	136

Cg1 and Cg2 are the centroids of rings C1-C6 and C8-C13 (Molecule 1), Cg3 and Cg4 are the centroids of rings C15-C20 and C22-C27 (Molecule 2).
Symmetry codes: (i) $-x, y-1/2, -z+3/2$; (ii) $-x, -y+2, -z+2$; (iii) $-x+1, -y+2, -z+1$; (iv) $x, -y+5/2, z-1/2$; (v) $-x+1, y+1/2, -z+3/2$.

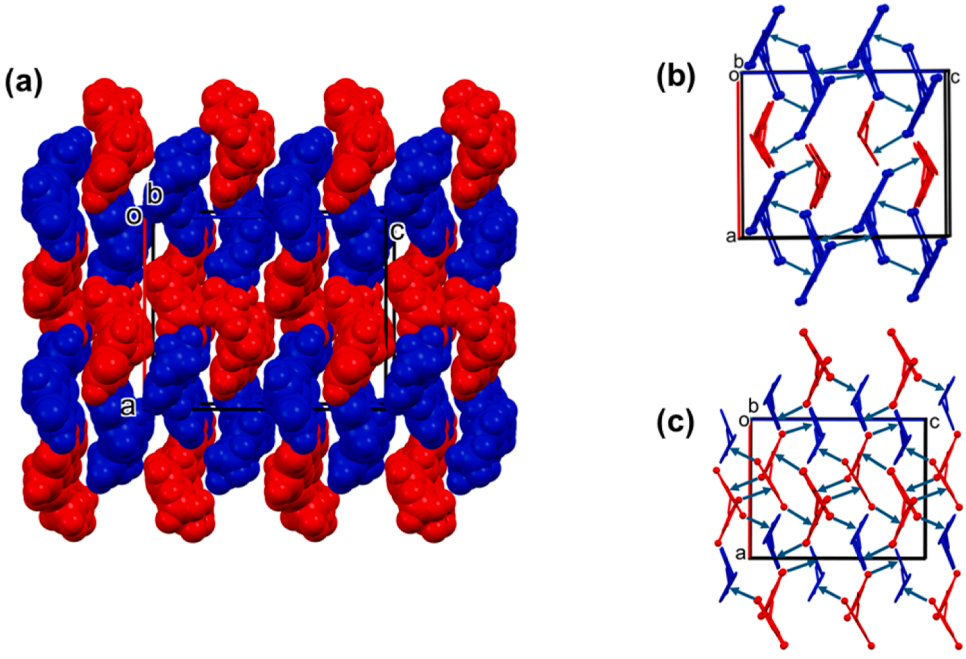

Fig. 2b. (a)The crystal packing of FBMA viewed along the *b*-axis direction. (space filling view; colour code: molecule 1 blue, molecule 2 red.), (b) a view along the *b*-axis of the 3 C—H…π interactions (green arrows) involving the H atoms of molecule 1 (blue balls), and (c) a view along the *b*-axis of the 4 C—H…π interactions (green arrows) involving the H atoms of molecule 2 (red balls).

Table 3
A comparison of selected crystallographic details and physical properties of various N-benzylideneaniline (NBA) Schiff bases.

Part 1 Compound name	FBMA	FBMOA	CBMOA	BBMOA
	Present work	Present work	[20]	[21]
Crystal system	Monoclinic	Monoclinic	Orthorhombic	Orthorhombic
Space group	$P2_1/c$	Cc	$Pna2_1$	$Pca2_1$
NMR, C = N (ppm)	8.474	8.487	8.423	8.44
FTIR, n(C = N) cm^{-1}	1626	1639	1613	1623
TPA, Z scan (m/W)	2.59×10^{-10}	9.8×10^{-12}	0.3×10^{-12}	1.3×10^{-12}
DTA, m.p. (°C)	73	93.6	151.7	145
TGA, Stability (°C)	230	180	177	160
Part 2				
Compound name	BBBA	DEABFA	DEABMOA	
	[11]	[12]	[14]	
Crystal system	Orthorhombic	Monoclinic	Triclinic	
Space group	Pccn	$P2_1$	P-1	
NMR, C = N (ppm)	8.364	8.261	8.30	
FTIR, n(C = N) cm^{-1}	1630	1627	1603	
TPA, Z scan (m/W)	1.3×10^{-11}	1.0×10^{-11}	—	
DTA, m.p. (°C)	145	decomposes	104	
TGA, Stability (°C)	200	—	210	

NMR- Nuclear Magnetic Resonance; FTIR – Fourier Transform Infrared; TPA – Two Photon Absorption; DTA – Differential Thermal Analysis; TGA- Thermogravimetric Analysis.

illustrated in Figure 2b(b), and that for the second group of 4 C—H…π interactions is illustrated in Fig. 2b (c).When combined these seven C—H…π interactions link the molecules to form a three-dimensional framework.

The differing substituents, notably OCH_3*cf*. CH_3, do not contribute to a variation in the solid-state packing arrangements; essentially C—H…π interactions leading to the formation three-dimensional frameworks. The presence of electron-withdrawing groups (F, Cl and Br) on the benzylidene ring of the three derivatives, F/Cl/Br-BMOA, reduces the electron density distribution within the molecules, which hinders their ability to engage in π-π interactions with neighbouring molecules.

It is interesting to note that the similar methoxyaniline substituted compounds, CBMOA [21] and BBMOA [22], crystallize in the orthorhombic system adopting space groups $Pna2_1$ and $Pca2_1$, respectively, while FBMOA crystallizes in the monoclinic crystal system adopting the Cc space group. These4'-methoxy-aniline compounds all crystallize in noncentrosymmetric space groups (Table 3). FBMA, the 4′-methyl-aniline compound crystallizes as a twin in the monoclinic system but with a centrosymmetric space group ($P2_1/c$) and two independent molecules in the asymmetric unit.

3.2. Hirshfeld surface analysis

The Hirshfeld surface and interactions of neighbouring molecules are presented in Fig. 3a (FBMOA) and Fig. 3b (FBMA). Short interatomic C—H…F contacts of FBMOA are represented by the red spots. The two-dimensional fingerprint plots show the estimated percentage contribution of nearby interactions, with major contributions from H…H, C…H/H…C, F…H/H…F, O…H/H…O and N…H/H…N contacts; shown in Figure4a (FBMOA) and Figure4b (FBMA). For FBMOA the most important interatomic contacts are identified as C…H/H…C (38%), that appear as two wing-like shapes highlighting their significant contribution to the overall stability of the crystal. The second most prominent interatomic contact is H…H (34.1%). For FBMA (Fig. 4b), H…H interactions are the most prominent (42.7%) while C…H/H…C interactions are the second most prominent interatomic contacts (31.6 %), followed by the F…H/H…F contacts that contribute 19%.

A comparison of relative percentage contributions of interatomic interactions to the Hirshfeld surfaces of FBMOA, CBMOA, BBMOA and FBMA are given in Fig. 5. Interatomic interactions of CBMOA and BBMOA such as H…H (34.6% *cf*. 34.5%) and N…H/H…N (5.5%) show close contributions. C…H/H…C and the O…H/H…O interactions of the FBMOA contribute 38% and 6.5%, respectively, which are slightly higher when compared to the respective values for CBMOA (36.7% and 4%) and BBMOA (36.3% and 3.9%). F/Cl/Br…H/H…F/C/Br and F/Cl/Br…O/O…F/Br/Cl interactions of FBMOA (13.9 and 1%) show slightly lower contributions than that of CBMOA (15.6 and 3.1%) and BBMOA (15.1 % and 3.1%). The relative contributions of H…F/F…H and N…H/H…N appear as 19 % and 5.6 % for FBMA. The presence of different substituents attached to the aromatic rings in these compound scan influence their interatomic interactions, ultimately affecting their solid-state packing and properties. However, this does not appear to be the case here as for all four compounds C—H…π interactions lead to the formation of three-dimensional frameworks.

3.3. Spectral analyses

The Fourier transform infrared spectra (400 – 4000 cm^{-1}) of FBMOA and FBMA are illustrated in Fig. 6. The strong stretching vibration of the imine bond (C = N) is observed at 1630 cm^{-1} for FBMOA and 1626 cm^{-1} for FBMA. The peaks at 1461 cm^{-1} and 1575 cm^{-1} in the FBMOA spectrum relate to aromatic C = C stretching vibrations. Similarly, the aromatic C = C stretching vibrations in FBMA are perceived at 1503 cm^{-1} and 1588 cm^{-1}. *Para* di-substituted C—H deformation modes appear at 842 cm^{-1} and 821 cm^{-1} for FBMOA and FBMA, respectively. The values observed conform to those observed previously for similar compounds [33].

3.4. Thermal analyses

TGDTA analyses of FBMOA and FBMA compounds are shown in Fig. 7. In the DTA diagram a sharp endothermic peak was observed at ~ 96 °C for FBMOA and at ~ 73 °C for FBMA, which correlate to the melting points of the compounds. Both compounds exhibit a single step weight loss in the TGA curve, and FBMOA undergoes bulk decomposition at ~ 180 °C and FBMA at ~230 °C. This indicates that FBMA exhibits a higher thermal stability compared to FBMOA.

3.5. Linear and nonlinear optical properties

Fig. 8a shows that FBMOA exhibits absorption peaks at 235 nm and 263 nm and FBMA (Fig. 8b) at 260 nm. They can be assigned to the π-π* transition involving the conjugated system of the aromatic rings. Absorption peaks at 331 nm (FBMOA) and 316 nm (FBMA) may be attributed to n-π* transition of these compounds.

The Z-scan curves obtained for FBMOA (Fig. 9a) and FBMA (Fig. 9b) solutions show smooth valleys that are symmetric about the focal point, indicating enhanced absorption at higher optical intensities. The nonlinear absorption coefficient (β) values were calculated from the best-fit curves of Eqn. (1) to the measured Z-scan data and were found to be 9.8×10^{-12}m/W for FBMOA and 2.59×10^{-10} m/W for FBMA. When comparing FBMOA with CBMOA (0.3×10^{-12}m/W) and BBMOA (1.3 10^{-12}m/W), it can be seen that the presence of the fluoro group contributes to its high nonlinearity due to its high electron affinity. FBMA shows higher nonlinearity compared to FBMOA (2.59 10^{-10}m/W). The

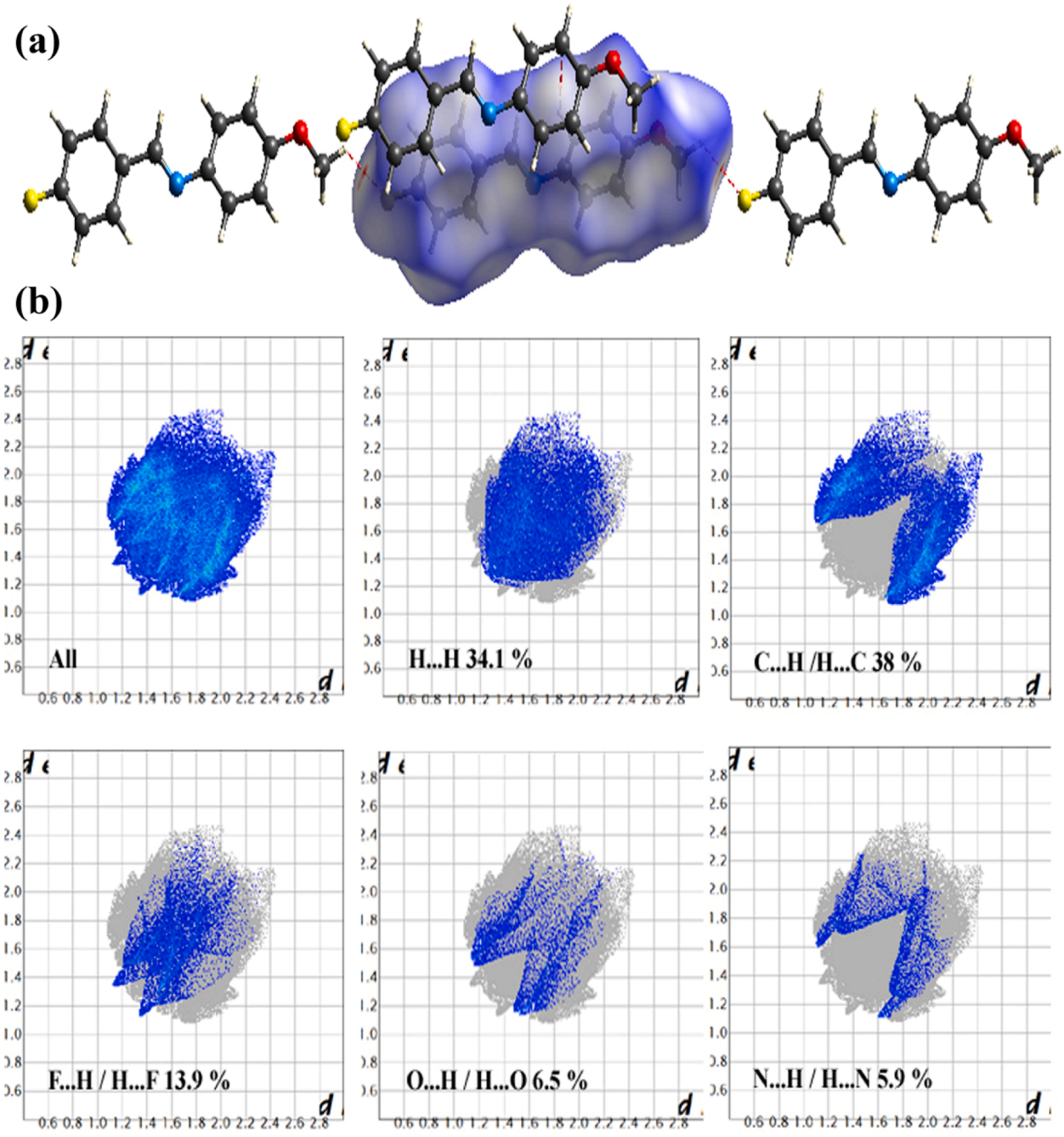

Fig. 3. (a) Hirshfeld surface of FBMOA mapped over d_{norm}, and (b) the full 2D fingerprint plot for FBMOA, and those delineated into H…H, C..H/H…C, F…H/H…F, O…H/H…O and N…H/H…N contacts.

presence of a methyl group in FBMA may affect the electron density distribution and conjugation in the molecule when compared to the methoxy group in FBMOA. This difference in electronic structure may lead to variations in nonlinear optical properties.

In Table 3, various characteristics of the title compounds and some related NBAs, such as 4-bromo-N-(4-bromorbenzylidene)anailene (BBBA) [11], 4-fluoro-N-[4-diethylamino)benzylidene]aniline (DEABFA [12] and N,N-diethyl-4-{[(4-methoxyphenyl)imino]methyl}aniline (DEABMOA) [14], and CBMOA and BBMOA, are compared. It can be seen that NBA Schiff base compounds with a common structural backbone, but with different substituents on the aromatic rings and different side chains have distinct physiochemical characteristics.

4. Conclusions

Compounds 4-fluorobenzylidene-4-methoxyaniline (FBMOA) and 4-fluorobenzylidene-4-methylaniline (FBMA) were successfully synthesized through a condensation reaction and crystals were grown by the slow evaporation method. FBMOA forms crystals in the non-centrosymmetric space group Cc, whereas FBMA forms crystals in the centrosymmetric space group $P2_1/c$, with two independent molecules in the asymmetric unit. Hirshfeld surface analysis revealed that the major interatomic contacts involve C…H/H…C interactions for FBMOA and H…H interactions for FBMA. The FTIR spectral studies provide valuable insights into the functional groups present in the compound. TGDTA analyses substantiated the melting point and purity of the compounds,

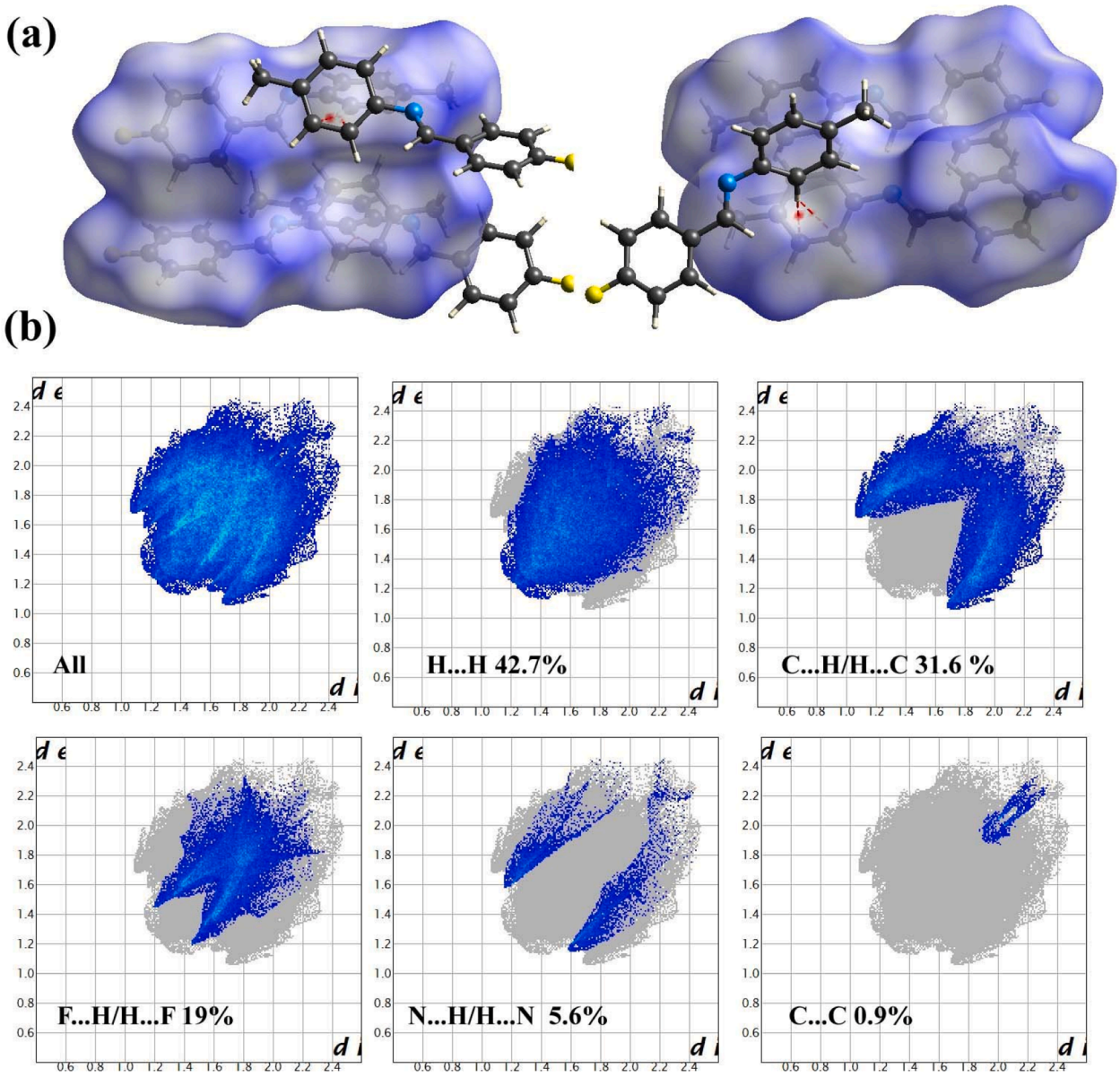

Fig. 4. (a) Hirshfeld surface of FBMA mapped over d_{norm}, and (b) the full 2D fingerprint plot for FBMA, and those delineated into H…H, C..H/H…C, F…H/H…F, N…H/H…N and C…C contacts.

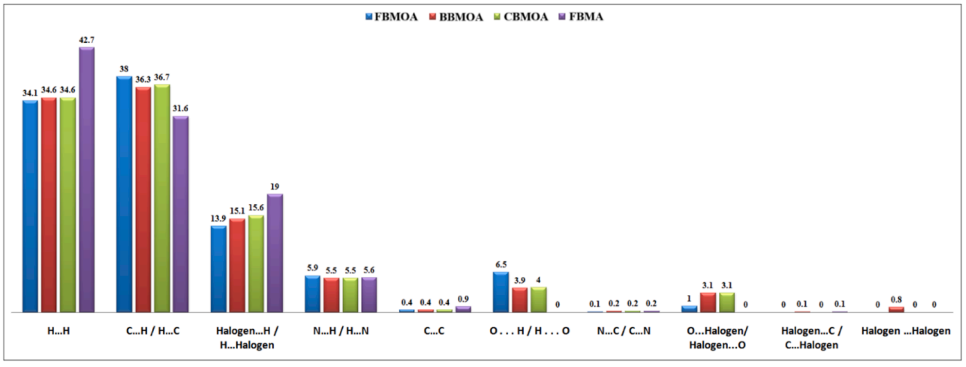

Fig. 5. A comparison of relative percentage contributions of interatomic interactions to the Hirshfeld surface of FBMOA, CBMOA, BBMOA and FBMA.

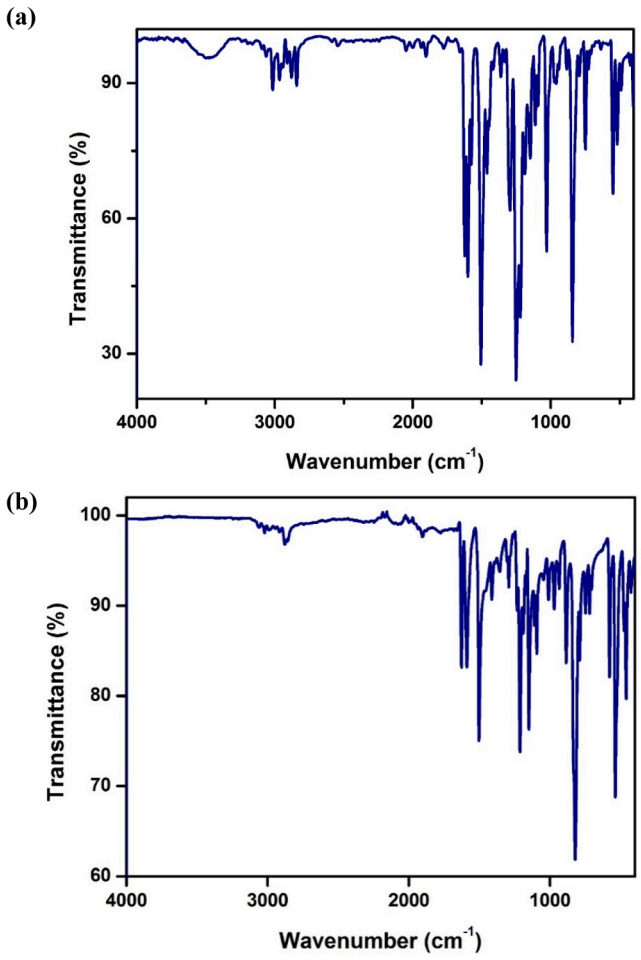

Fig. 6. FTIR spectra of (a) FBMOA and (b) FBMA.

ensuring their integrity for further investigations. The value of the nonlinear optical absorption coefficients indicates that compounds FBMOA and FBMA possess potential for future applications in nonlinear optical devices, such as optical limiters. These results contribute to a deeper understanding of these and similar compounds and lay the groundwork for their potential applications in various technological and scientific fields.

CRediT authorship contribution statement

A. Subashini: Writing – original draft, Methodology, Conceptualization. **R. Kumaravel:** Writing – review & editing, Investigation. **Helen Stoeckli-Evans:** Writing – review & editing, Validation. **T. Sabari Girisun:** Investigation. **Sharon Mary Tomson:** Investigation. **Reji Philip:** Investigation. **Aurelien Crochet:** Investigation. **R. Ramesh Babu:** Supervision. **K. Ramamurthi:** Supervision.

Declaration of competing interest

The authors declare that they have no known competing financial interests or personal relationships that could have appeared to influence the work reported in this paper.

Supplementary materials

Supplementary material associated with this article can be found, in the online version, at doi:10.1016/j.molstruc.2024.141121.

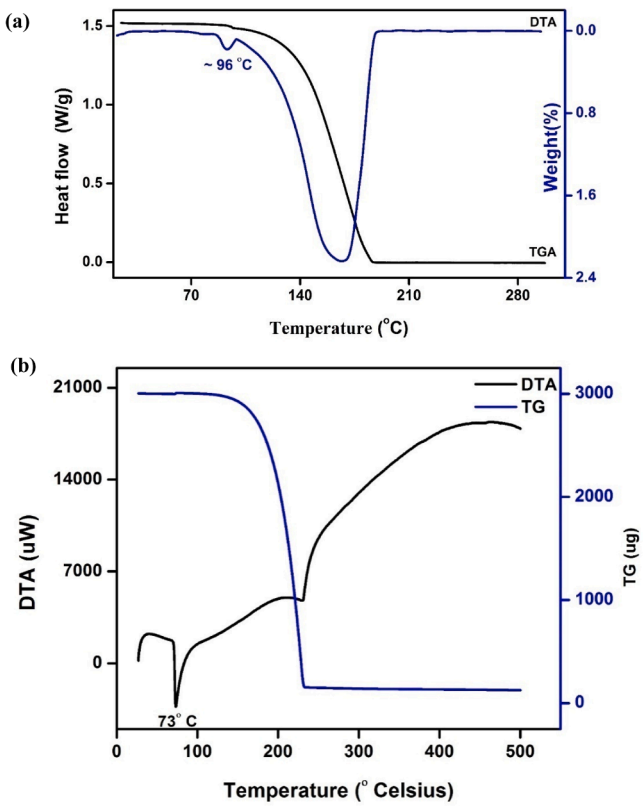

Fig. 7. TGA and DTA curves for (a) FBMOA and (b) FBMA.

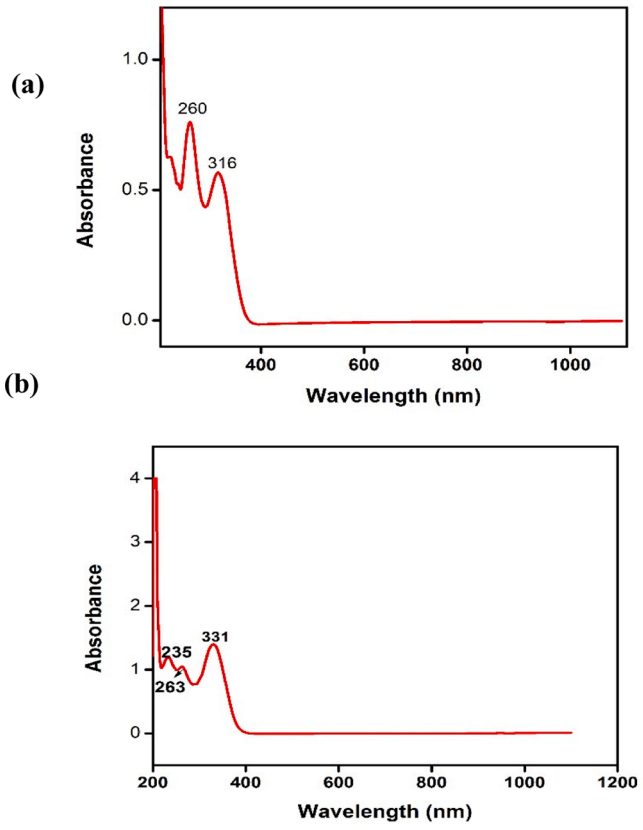

Fig. 8. Absorbance spectra of (a) FBMOA and (b) FBMA.

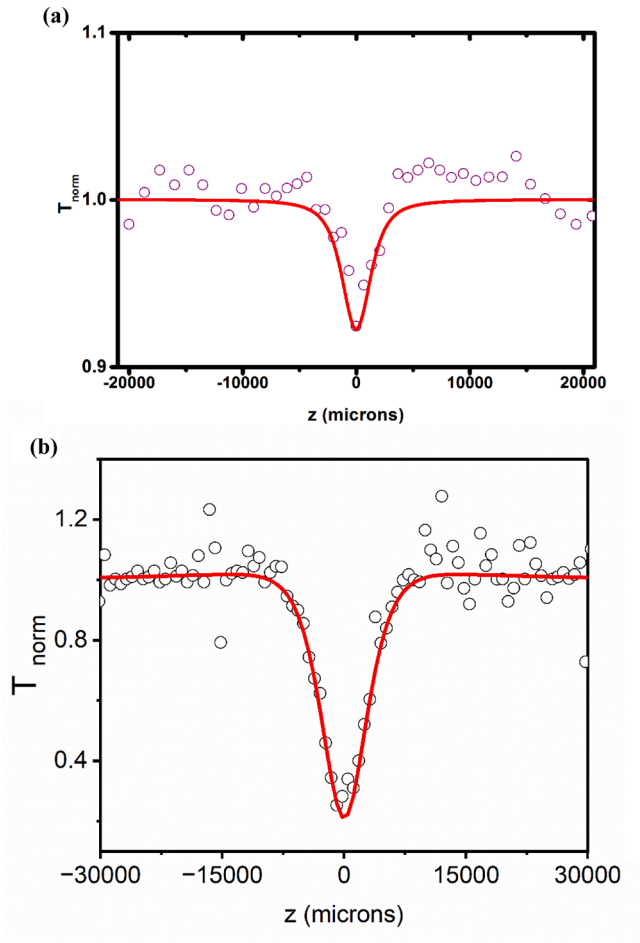

Fig. 9. Open aperture Z-scan curves of (a) FBMOA and (b) FBMA. Open circles are the experimental data points while the solid curves are the numerical fits to a two-photon absorption process calculated using Eqn.1.

Data availability

CCDC nos.940432 and 2376715 contain the supplementary crystallographic data for compounds FBMOA and FBMA, respectively. These data can be obtained free of charge from CCDC via https://www.ccdc.cam.ac.uk/conts/retrieving.html.

References

[1] S.J. Weishaupl, D.C. Mayer, Y. Cui, P. Kumar, H. Oberhofer, R.A. Fischer, J. Hauer, A. Pothig, J. Mater. Chem. C 10 (2022) 6912.
[2] J.K. Zareba, M. Nyk, M. Samoc, Adv. Opt. Mater. 9 (2021) 2100216.
[3] M. Mutailipu, M. Zhang, H. Wu, Z. Yang, Y. Shen, J. Sun, S. Pan, Nat. Commun. 9 (2018) 3089.
[4] M. Mutailipu, S. Pan, Angew. Chem. Int. Ed. Engl. 46 (2020) 20302.
[5] P.G. Lacroix, Eur. J. Inorg. Chem. (2001) 339, 2001.
[6] S. Tariq, M. Tahir, I. Shafiq, M. Saqib, S. Haq, H. Aftab, M. Imran, Z. Shafiq, J. Mol. Struct. 1308 (2024) 138135.
[7] I. Waziri, M.T. Kelani, M.O. Oyedeji-Amusa, A.K. Oyebamiji, L-C.C. Coetzee, A. S. Adeyinka, A.J. Muller, J. Mol. Struct. 1276 (2023) 134756.
[8] M.V. Chernysheva, M. Bulatova, X. Ding, M. Haukka, Cryst. Growth Des. 20 (2020) 7197.
[9] U. Grob, S. Rudiger, B. Bassner, H. Hagemann, J.C. Tatlow, Methods of Organic Chemistry (Houben-Weyl), in Organo-Fluorine Compounds, Thieme, Stuttgart, 4th ed, 1999.
[10] T. Hiyama, Organo Fluorine Compounds, Chemistry and Applications, Springer, Berlin, 2000.
[11] A. Subashini, K. Ramamurthi, R.Ramesh Babu, Reji Philip, Helen Stoeckli-Evans, Acta Cryst E79 (2023) 146.
[12] A. Subashini, Reji Philip, Helen Stoeckli-Evans, R. Ramesh Babu, K. Ramamurthi, J. Chem.Cryst. 53 (2022) 370.
[13] S. Leela, A. Subashini, Reji Philip, K. Ramamurthi, Helen Stoeckli-Evans, Acta Cryst E76 (3) (2020) 417.
[14] A. Subashini, R. Kumaravel, B. Tharmalingam, K. Ramamurthi, A. Crochet, Helen Stoeckli-Evans, Acta Cryst E80 (2024) 201.
[15] H. Yamaguchi, M. Kondo, T. Sasaki, M. Sakamoto, H. Ono, N. Kawatsuki, Langmuir 38 (2022) 2862.
[16] R. Verma, N. Pal Lamba, A. Dandia, A. Srivastava, K. Modi, M.S. Chauhan, J. Prasad, Sci. Rep. 12 (2022) 9636.
[17] R.M. Ramadan, M.M. Abo-Aly, A.A.M. Lasheen, Inorg. and Nano-Metal Chem. 53 (2023) 1306.
[18] A. Subashini, V. Veeramani, K. Thamaraiselvi, Aurelien Crochet, Priya Rose, Reji Philip, R. Ramesh Babu, K. Ramamurthi, Optic. Mater. 117 (2021) 111081.
[19] S. Leela, T. Deepa Rani, A. Subashini, S. Brindha, R. Ramesh Babu, K. Ramamurthi, Arabian J. Chem. 10 (2017) S3974.
[20] N.T. Subasi, Overview of Schiff Bases; Schiff Bases in Organic, Inorganic and Physical Chemistry. Ed. T. Akitsu. Intech Open, 2022. 10.5772/interopen.104134.
[21] X.-Y Ren, Y.-F. Ding, F.-F. Jian, Acta Cryst E64 (2008) o1793.
[22] R. Ma, Y. Hou, X. Yong, Y. Cen, Acta Cryst E63 (2007) o4188.
[23] Stoe, X-Area Cie, X-RED Software, Stoe & Cie GmbH (2009). Darmstadt, Germany.
[24] G.M. Sheldrick, ActaCryst A64 (2008) 112.
[25] G.M. Sheldrick, Acta Cryst C71 (2015) 3.
[26] A.L. Spek, Acta Cryst E76 (2020) 1.
[27] O.V. Dolomanov, L.J. Bourhis, R.J. Gildea, J.A.K. Howard, H. Puschmann, J. Appl. Cryst. 42 (2009) 339.
[28] L.J. Bourhis, O.V. Dolomanov, R.J. Gildea, J.A.K. Howard, H. Puschmann, Acta Cryst A71 (2015) 59.
[29] C.F. Macrae, I. Sovago, S.J. Cottrell, P.T.A. Galek, P. McCabe, E. Pidcock, M. Platings, G.P. Shields, J.S. Stevens, M. Towler, P.A. Wood, J. Appl. Cryst. 53 (2020) 226.
[30] P.R. Spackman, M.J. Turner, J.J. McKinnon, S.K. Wolff, D. J.Grimwood, D. Jayatilaka, M.A. Spackman, J. Appl. Cryst. 54 (2021) 1006.
[31] M. Kumar, S. Perumbilavil, D.R. Vinaakumara, A. Goel, R. Philip, S. Kumar, ACS Omega 48 (2023) 45961.
[32] C.R. Groom, I.J. Bruno, M.P. Lightfoot, S.C. Ward, Acta Cryst B72 (2016) 171–179.
[33] M. Silverstein, X. Webster, J. Kiemle, Spectrometric Identification of Organic Compounds, Wiley, New York, 2005.